Research Article | Vol. 30, No. 6 / 14 Mar 2022 / Optics Express 8560
Optics EXPRESS

Mid-infrared silicon-on-insulator waveguides with single-mode propagation over an octave of frequency

CALLUM J. STIRLING,* WEI CAO, JAMIE D. REYNOLDS, ZHIBO QU, THOMAS D. BRADLEY, LORENZO MASTRONARDI, FREDERIC Y. GARDES, AND MILOS NEDELJKOVIC

Optoelectronics Research Centre, Zepler Institute for Photonics and Nanoelectronics, University of Southampton, University Road, Southampton, SO17 1BJ, UK
*c.stirling@soton.ac.uk

Abstract: Increasing the working optical bandwidth of a photonic circuit is important for many applications, in particular chemical sensing at mid-infrared wavelengths. This useful bandwidth is not only limited by the transparency range of waveguide materials, but also the range over which a waveguide is single or multimoded for predictable circuit behaviour. In this work, we show the first experimental demonstration of "endlessly single-mode" waveguiding in silicon photonics. Silicon-on-insulator waveguides were designed, fabricated and characterised at 1.95 µm and 3.80 µm. The waveguides were shown to support low-loss propagation (1.46 ± 0.13 dB/cm loss at 1.95 µm and 1.55 ± 0.35 dB/cm at 3.80 µm) and single-mode propagation was confirmed at 1.95 µm, meaning that only the fundamental mode was present over the wavelength range 1.95 - 3.80 µm. We also present the prospects for the use of these waveguides in sensing applications.

1. Introduction

For many photonic integrated circuits (PICs), single-mode propagation is a requirement of the waveguides for predictable optical behaviour. However, for a conventional rib or strip waveguide, the wavelength range for solely supporting the fundamental mode is limited. This is exemplified in Fig. 1 which shows the effective indices of the first three transverse electric/magnetic (TE/TM) modes for a strip waveguide. Waveguide modes are considered guided if their effective index is above the refractive index of the waveguide cladding at a given wavelength. For effective indices below this cut-off, the modes can couple into the cladding modes and will be radiative. Therefore, for single-moded guidance, the higher order modes must have an effective index above this cut-off value. As demonstrated by Fig. 1, for a given waveguide cross-section, at shorter wavelengths the waveguide is multimoded, while at longer wavelengths the waveguide ceases to be guiding, thereby limiting the wavelength range for single-moded guidance.

The limited bandwidth of single-mode propagation is a significant issue for some applications in the mid-infrared (MIR) wavelength range, where a PIC may need to have a working optical bandwidth larger than a typical rib or strip waveguide can support. MIR absorption spectroscopy can require chemicals to be differentiated by measuring multiple absorption peaks across a wide wavelength range. For example, the MIR "fingerprint region" covers the wavelength range λ = 8 - 20 µm [1], i.e. more than an octave of frequency. Even when examining narrow spectral features, it would be desirable to be able to use the same PIC to measure different analytes with absorption features at vastly different wavelengths, so that the same chips could be used for multiple practical applications without requiring redesign and re-fabrication. This is especially important since

#448284 https://doi.org/10.1364/OE.448284
Journal © 2022 Received 10 Nov 2021; accepted 6 Dec 2021; published 1 Mar 2022

Optics EXPRESS

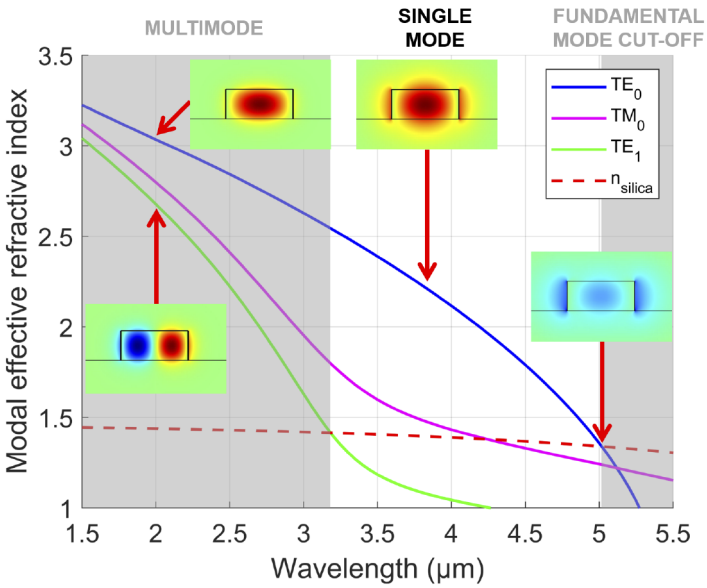

Fig. 1. Effective indices of the first three supported modes in a SOI strip waveguide, with 1.2 μm width and 500 nm height, simulated in Lumerical MODE Solutions. Inserted images show the electric field of the TE modes at the wavelengths indicated by the red arrows. For effective index values below the refractive index of the SiO_2, the waveguide modes are radiative. The grey-shaded areas indicate wavelength regions where the waveguide is not single-mode.

group-IV photonics technologies can only achieve low-cost fabrication when manufactured in high volumes, and the markets for individual sensing applications may be small.

The need for waveguides with a wide single-moded bandwidth can be illustrated by considering a particular device, such as a Fourier-transform spectrometer [2]. When higher order modes are excited in a waveguide, their beating will form an interference pattern, so that the waveguides exhibit a wavelength dependent transmission. In a spectrometer based on a Mach-Zehnder interferometer it would create an unpredictable optical time delay for light travelling through the two waveguide arms. It would effectively introduce frequency dependent errors into the power spectral density measurement, limiting the achievable resolution and therefore restrict the sensitivity of the device.

Beyond early efforts in establishing a condition for single-moded guidance based on the waveguide geometry [3,4], surprisingly little effort has been made to actually find the single-moded bandwidth of various waveguide designs. Most authors in literature either rely on the aforementioned single-mode condition or simply find the waveguide geometry using numerical solvers that supports only the fundamental mode for their specific wavelength of interest.

Endlessly single-mode (ESM) waveguide designs have previously been proposed for both silicon-on-insulator (SOI) and a SOI/III-V hybrid platform [5], inspired by the well-known ESM photonic crystal fibre [6]. Rather than using a step-index cladding, in this design the lateral waveguide cladding is patterned as a grating, with the "grooves" and "teeth" of the grating parallel to the waveguide core; the grooves are filled with an effective material, with an index that can be controlled by patterning on a sub-wavelength scale (see Fig. 2). Since the cladding consists of a grating that is solely silicon and air, the cladding mode for this waveguide has a comparatively high propagation constant, and therefore also effective index. Furthermore, the effective index of the cladding mode increases at shorter wavelengths where it becomes more

Optics EXPRESS

concentrated within the silicon teeth of the grating, thereby preventing the emergence of higher order modes. The lack of a sharp index change means that, at longer wavelengths where the mode area is larger, the mode is not squeezed out of the waveguide and confinement within the silicon core is maintained, meaning that it is still guided.

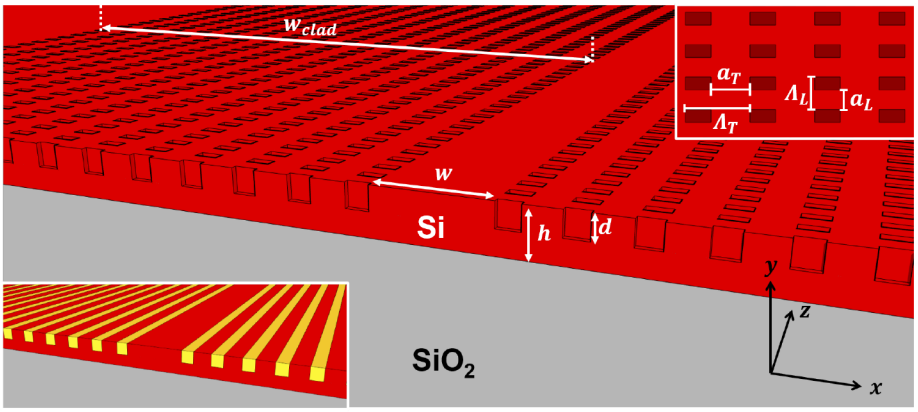

Fig. 2. Three-dimensional illustration of a fabricated ESM waveguide, with the labelled design parameters. [top inset] top-view of a section of the sub-wavelength grating cladding. [bottom inset] the sub-wavelength regions of the wavelength cladding, approximated as a homogenous material with index $\boldsymbol{n}_{\mathrm{SWG}}$ (in yellow).

Although these waveguides were predicted to be single-moded across 1.1 - 5 μm in simulations [5] (i.e. the whole transparency range of SOI), they have not been experimentally demonstrated in silicon photonics. In this work, we show the optical characterisation of a similar waveguide design based solely in SOI, that supports single-mode propagation over an octave of frequency. Furthermore, although the absorption from the underlying SiO_2 layer limits the use of SOI at longer MIR wavelengths, the waveguide design approach that we experimentally demonstrate here could be adapted for use in other group IV material platforms, for $\lambda > 4$ μm.

2. Design

The design of the ESM waveguides used in this work is shown in Fig. 2, for an SOI platform. A waveguide with core width w is defined by a two-dimensional grating, to act as the cladding. The longitudinal period of the grating, Λ_{L}, is small enough so that the grating is subwavelength in the z-direction (i.e. the period is smaller than the Bragg period [7]) and can be modelled as an homogeneous anisotropic material, so the cladding is effectively a one-dimensional grating in the transverse direction with period Λ_{T} (see bottom insert of Fig. 2). The size of the silicon grating teeth in the longitudinal and transverse directions are a_{L} and a_{T} respectively.

By varying the duty cycle of the subwavelength regions of the grating, the refractive index of the effective homogeneous material (and consequently the cladding index) can be tuned to ensure single-mode propagation across a wide bandwidth. When the subwavelength regions of the grating are treated as a homogenous material, they are considered to have a refractive index tensor $\boldsymbol{n}_{\mathrm{SWG}}$ [8]:

$$\boldsymbol{n}^2_{\mathrm{SWG}} = \begin{bmatrix} n^2_{xx} & 0 & 0 \\ 0 & n^2_{yy} & 0 \\ 0 & 0 & n^2_{zz} \end{bmatrix} \tag{1}$$

Optics EXPRESS

where n_{xx}, n_{yy} and n_{zz} are the refractive indices in the x-, y- and z-directions respectively. For structure in Fig. 2, in the deep sub-wavelength regime (i.e. $\lambda \gg \Lambda_L$) each of these indices can be approximated using Rytov's formulae [9]:

$$n_{xx}^2 \sim \frac{a_L}{\Lambda_L} \cdot n_{Si}^2 + \left(1 - \frac{a_L}{\Lambda_L}\right) \cdot n_{air}^2; \tag{2}$$

$$n_{yy}^2 = n_{xx}^2; \tag{3}$$

$$\frac{1}{n_{zz}^2} \sim \frac{a_L}{\Lambda_L} \cdot \frac{1}{n_{Si}^2} + \left(1 - \frac{a_L}{\Lambda_L}\right) \cdot \frac{1}{n_{air}^2}, \tag{4}$$

where n_{Si} and n_{air} are the refractive indices of silicon and air respectively.

The waveguide structure was modelled in Lumerical MODE solutions to determine the grating parameters that would ensure single-mode propagation across $\lambda = 1.5 - 5.5$ µm. Perfectly matched layer boundary conditions were used so that optical power was allowed to leave the simulation region, meaning that leaky modes would not be found by the simulator. Using the dimensions in [5] as a starting point for the simulation, with $n_{zz} = 1.5$ (achievable with a longitudinal duty cycle $a_L/\Lambda_L = 0.6$), $\Lambda_T = 600$ nm and a transverse duty cycle $a_T/\Lambda_T = 0.5$. Note that as the eigenmode solver is two-dimensional, the longitudinal grating dimensions were only input into the simulation as a duty cycle, to yield n_{zz}. The waveguides were designed for an SOI platform with $h = 500$ m and the grating holes etched halfway through the silicon layer, i.e. $d = 250$ nm. The core width was fixed as $w = 1.2$ µm, as this was found to be sufficient to support the fundamental mode in a conventional waveguide over $\lambda = 1.5 - 5$µm so it was expected that this would be sufficient for the ESM waveguide also (see Fig. 1). The critical parameters (both duty cycles, the transverse period and the etch depth) were varied over the wavelength range to find the solution in which fundamental mode had the largest effective index (indicative

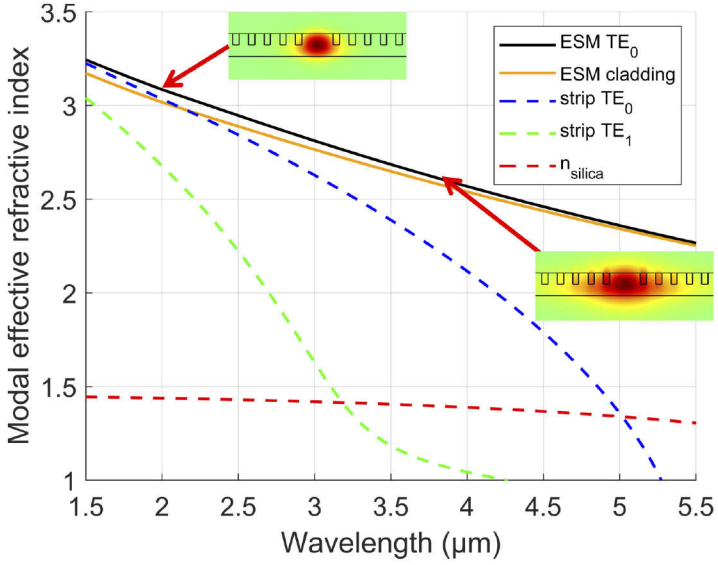

Fig. 3. Effective indices of the fundamental TE mode and the TE cladding mode for the ESM waveguide. Inserted images show the electric field of the TE_0 mode at the wavelengths indicated by the red arrows. For comparison, the effective indices of the first two TE modes for an SOI strip waveguide with the same core size (the same as in Fig. 1) and the refractive index of SiO_2 are also shown.

Optics EXPRESS

of confinement within the waveguide) and with no other modes supported in the waveguide. The best solution found only the fundamental TE mode (not even the fundamental TM mode) was supported over the entire simulated wavelength range, with $\Lambda_T = 600$ nm, $d = 250$ nm and $a_T/\Lambda_T = a_L/\Lambda_L = 0.6$.

The modal analysis for the ESM waveguide is shown in Fig. 3, alongside the modal analysis for a conventional strip waveguide with the same core cross-sectional area. The effective index of the ESM cladding mode was found by simulating the ESM structure without the waveguide core in an eigenmode solver with metal boundary conditions (as the cladding mode would be leaky) over the same wavelength range. From Fig. 3, the principle of the ESM waveguides is evident; the large index of the cladding mode prevents any higher order modes from being supported across this wavelength range. Furthermore, comparison of the TE_0 modes for both the ESM and conventional waveguides shows that, for the ESM waveguide, the TE_0 mode has a greater confinement within the waveguide core across the wavelength range.

3. Results and discussion

Since the simulation did not yield an optimal value of the longitudinal period, it was selected as $\Lambda_L = 300$nm, as this was below the Bragg period and would give the critical dimension for the hole size as 120 nm, facilitating fabrication by electron beam lithography. The transverse grating was repeated for 16 periods, for a cladding width $w_{clad} = 9.6$ µm. To experimentally demonstrate that the waveguides were single-moded over a broad wavelength range, the waveguides were experimentally characterised at $\lambda = 1.95$µm and $\lambda = 3.80$µm, covering an octave of frequency. The values of the resulting refractive indices of the homogenised subwavelength regions at each of these wavelengths are shown in Table 1. The TE_0 mode profiles for these wavelengths are shown in Fig. 3.

Table 1. Refractive index values for the homogenous anisotropic sub-wavelength regions of the cladding grating at the characterisation wavelengths.

Wavelength, λ (µm)	n_{xx} (= n_{yy})	n_{zz}
1.95	2.7469	1.4901
3.80	2.7269	1.4888

The waveguides were fabricated on a 500 nm SOI sample, by patterning with a JEOL JBX-9300FS electron beam lithography tool and ZEP-520A photoresist, and etching in an Oxford Instruments ICP 380 plasma system. A scanning electron microscope (SEM) image of the fabricated waveguide is shown in Fig. 4.

Two sets of waveguides were fabricated simultaneously on the the same sample, with grating coupler and tapers for the optical input and output. Over the grating coupler region, the waveguide core had a width of 10 µm to enable easy fibre alignment and this width was tapered down to 1.2 µm over 1 mm; in the taper, the sub-wavelength holes in the waveguide cladding were angled to run parallel to the waveguide edges. In both sets, the waveguide design was identical but a different grating coupler design was used for each measurement wavelength. Note that grating couplers were used to facilitate easy characterisation in this case, but in a real device, broadband inputs such as edge-coupled or on-chip sources could be used. Within each set, the propagation loss of the waveguide design was determined using the cut-back method with waveguide lengths spanning 0.15 - 1.5 cm in 0.15 cm intervals. The waveguide transmissions in each set were normalised to the corresponding shortest waveguide in that set, as the different grating coupler designs would have different insertion losses.

Optics EXPRESS

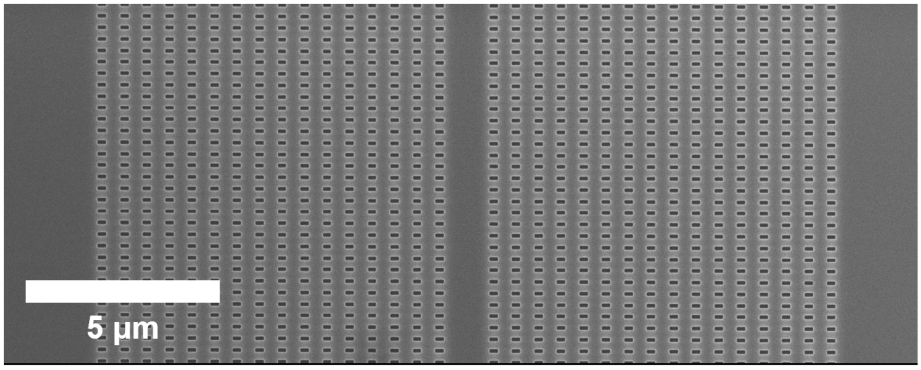

Fig. 4. Top-view SEM image of the fabricated ESM waveguide.

The propagation loss measurements were performed at 1.95 µm using a Thorlabs TLK-L1950R tunable laser (centred at 1.95 µm, tunable over 1.89 - 2.02 µm) and a Thorlabs PDA10DT-EC InGaAs photodetector (sensitive from 0.9 - 2.57 µm). The light launched into the waveguides was TE-polarised using a polarisation controller. Likewise, at 3.80 µm, the measurements were performed with a Daylight Solutions quantum cascade laser (QCL), tunable over 3.72 - 3.90 µm, and a liquid nitrogen-cooled InSb detector (InfraRed Associates Inc. IS-1.0, sensitive 1.0 - 5.5 µm). A half-wave plate was used for polarisation control, to ensure a TE-polarised input. For both setups, the laser was coupled into a fibre and fibre-to-chip coupling was achieved using the grating couplers.

The results of the waveguide propagation loss measurements are shown in Fig. 5; the propagation loss was determined to be 1.46 ± 0.13 dB/cm and 1.55 ± 0.35 dB/cm at 1.95 µm and 3.80 µm respectively. In both cases, not only does this demonstrate that the waveguides support propagation at both wavelengths, but also that the propagation loss is comparable to that of other silicon-based waveguides at these wavelengths [10–15], showing that the cladding does not introduce significant additional loss.

In order to confirm single-mode propagation, the waveguides used for the propagation loss measurements were cleaved to remove the output grating and associated taper, exposing the waveguide end facet and allowing the waveguide output to be imaged with an infrared (IR) camera. The same setup used for the loss measurements at 1.95 µm was used, replacing the output fibre and photodetector with a 63× objective lens (to expand the output) and the IR camera (Xenics Xeva 1.7 320, with 320×256 pixel focal plane array and 30 µm pixel pitch). One or more reflective neutral density filters was placed in the beam path to prevent damage to the IR camera from high optical power.

The waveguide outputs were only imaged around 1.95 µm because the longer wavelength (3.80 µm) was outside of the sensitivity range of the IR camera. However, confirming the absence of higher order modes at 1.95 µm would be sufficient to demonstrate that the waveguides would be single-moded across 1.95 - 3.80 µm. In general, for a waveguide with a given cross-section, it would be expected that a greater number of higher order modes would be supported when a shorter wavelength of light is propagated, than for a longer wavelength. Therefore, demonstration of solely single-mode propagation at the shorter wavelength would indicate that the waveguide is also single-moded at the longer wavelength, provided that waveguide still allows transmission at the longer wavelength.

To observe the evolution of the waveguide output with wavelength, the wavelength was swept in 0.5 nm steps and an image of the output was recorded at each step. For comparison, strip waveguides that were simulated to be single-mode (0.45 µm width, 500 nm height) and multimode

Optics EXPRESS

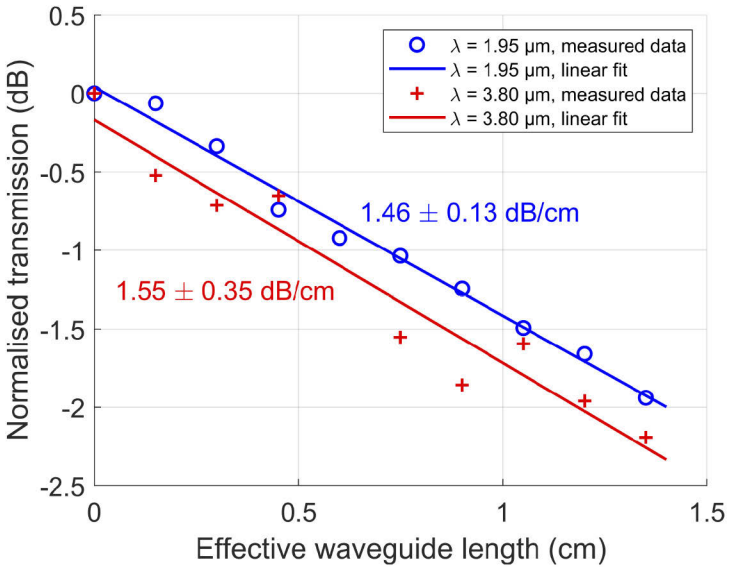

Fig. 5. Waveguide cut-back propagation loss measurements for ESM waveguides with the same design at 1.95 μm and 3.80 μm. The transmission measurements are normalised to the transmission through the shortest waveguide (0.15 cm) in each set. The quoted uncertainties in the propagation losses are the 95% confidence interval of the linear fits.

(1.2 μm width and 500 nm height) were also fabricated on 500 nm SOI samples, in the same way as the ESM waveguides. The simulated profiles of each of the TE modes supported by these two waveguides are shown in Fig. 6. These strip waveguides were also measured in the same way and their outputs were imaged at each wavelength step.

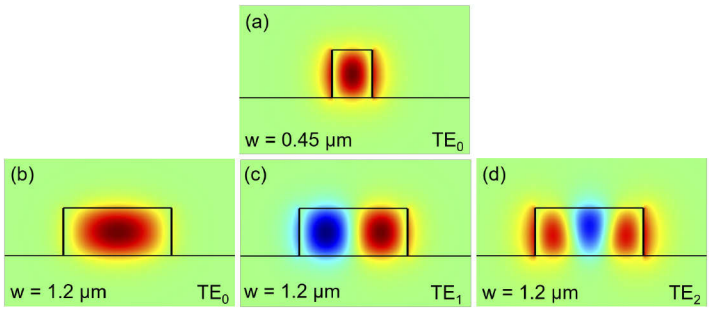

Fig. 6. The electric field of (a) the fundamental TE mode a single-mode strip waveguide (0.45 μm width) and (b)-(d) the first three guided TE modes of a multimode strip waveguide (1.2 μm width), simulated in Lumerical MODE Solutions at $\lambda = 1.95\ \mu$m. Both waveguides have a height of 500 nm.

For a given wavelength, a captured frame of the imaged outputs gives a measure of the output intensities $I(x, y)$. For each wavelength, the pixel intensities of the corresponding image were summed in the y-direction to give the intensity profile in the x-direction only, $I(x)$. These were then plotted consecutively to create a "heat map" of the evolution of the intensity profile with wavelength $I(x, \lambda)$, as shown in Fig. 7(a), Fig. 7(b) and Fig. 7(c) for the ESM, single-mode and multimode waveguides respectively.

Optics EXPRESS

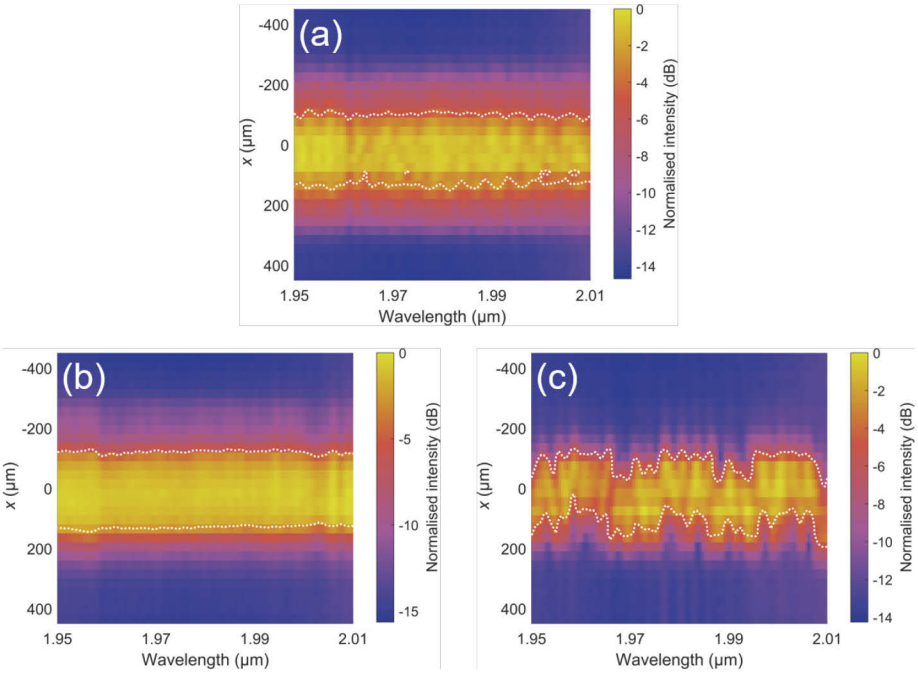

Fig. 7. The heat maps of the output intensity, as a function of pixel position and wavelength, are shown for the (a) ESM, (b) single-mode and (c) multimode waveguides. The intensity values are normalised to the largest pixel intensity of each heat map. The white dotted line shows the −3 dB contour for the heat map.

In Fig. 7(a), the overall intensity of the ESM waveguide output remains centrally located throughout the wavelength sweep, with some intensity fluctuations at the output edges attributed to background noise. This is comparable to the single-mode waveguide in Fig. 7(b), where the output intensity also has no movement in the x-direction with wavelength (the noise is less evident here, as the signal-to-noise ratio was larger for this waveguide). However, for the output of the multimode waveguide in Fig. 7(c), the intensity has a significant lateral shift (in the x-direction), much larger than any noise fluctuations. This is an indicator of multimode interference: in addition to the fundamental mode, higher order modes in the waveguide have been excited and they interfere with the fundamental mode. As the wavelength is swept, the relative phase between these modes changes, resulting in the observed interference pattern where the peak intensity (highlighted by the −3 dB contour) oscillates periodically in the lateral direction. The lack of significant lateral shift of the intensity for the ESM and single-mode waveguides indicates that no interference pattern is formed and, consequently, that no higher modes are supported in this wavelength range. Thus, it can be concluded that the ESM waveguide does indeed only support the fundamental mode at 1.95 μm and, since the same waveguide has been confirmed as guiding at 3.80 μm, it therefore follows that the ESM waveguide will also only allow single-mode propagation at 3.80 μm. Further, it is notable that the ESM and multimode waveguide cores are both 1.2 μm wide and 500 nm thick, so the lack of higher modes suggests that they are being suppressed by the cladding design, rather than simply being avoided with a suitable waveguide geometry.

Optics EXPRESS

4. Prospects for ultra-wideband PICs exploiting ESM waveguides

The obvious question for future research is: how could low loss PICs be created that exploit the full single-mode bandwidth of these ESM waveguides? Each individual component in such a circuit must have low fundamental mode loss in a broad operating range. As an example, Fig. 8 shows a simple circuit for homodyne absorption spectroscopy using an external tunable laser, in which light is coupled into the chip, split into sensor and reference waveguides, and then waveguide integrated detectors are placed at the end of each waveguide.

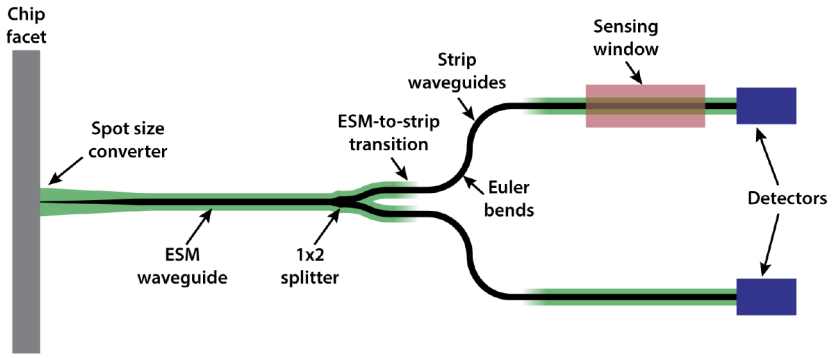

Fig. 8. Illustration of simple broadband PIC-based sensor.

The following passive components would need to be developed to achieve such a circuit.

a). Fibre-chip couplers: In this work we have used two different grating couplers to couple light into the ESM waveguides at different wavelengths. However, grating couplers have fundamentally narrow bandwidths due to their phase matching requirements. End-fire coupling using spot size converters that adiabatically convert the fibre mode into the fundamental waveguide mode are better candidates for broadband coupling. In the near-IR several very efficient and broadband edge couplers based on different kinds of inverse tapers have been proposed or demonstrated [16].

b). Waveguide bends: the low contrast between the indices of the ESM fundamental and cladding modes suggests that the bending loss of the ESM waveguide will be quite large—this is a known limiting factor for the photonic crystal fibre [17], on which this design is inspired. This is confirmed by three-dimensional (3D) finite-difference time-domain (FDTD) bending loss simulations of the waveguide, where at even fairly large bend radii the loss is significant, as shown in Fig. 9. Fortunately, within integrated photonics (unlike in fibres) there may be design approaches to overcome this limitation. For example, one approach may be to use multimode strip waveguides for the bends to increase the lateral mode confinement and decrease the bend radius. In this case the structure will need to be carefully designed so that higher order modes are not excited. To do this, adiabatic transitions between the ESM and multimode waveguides can be used in combination with a bend shape with gradually changing curvature, such as Euler bends [18].

c). Beam splitters: Several solutions exist for broadband waveguide splitting in SOI. 1×2 Y-junctions that were numerically optimised for broadband mid-IR operation [19] have been shown to have <0.3dB insertion loss over at least 2.8-3.7 μm in simulations and 3.2-3.7 μm experimentally. In the near-IR "wavelength agnostic" 1×2 beamsplitters that rely on mode engineering have been shown with <1dB insertion loss over at least 1260-1650nm [20]. Both of these work by gradually transforming one mode into two, which fundamentally has

Optics EXPRESS

a weak dependence on wavelength. Further work is needed to integrate such splitters with ESM waveguides and to confirm whether they can exhibit low loss over the octave spanning wavelength range explored here. Where 2×2 beamsplitters are required (e.g. for switching) it will be more challenging to achieve such broadband operation, but wideband multimode interferometers have been demonstrated with <1 dB insertion loss and imbalance over the 3.1-3.7 μm range [21] by implementing the multimode section of the device using a subwavelength grating with an anisotropic effective refractive index.

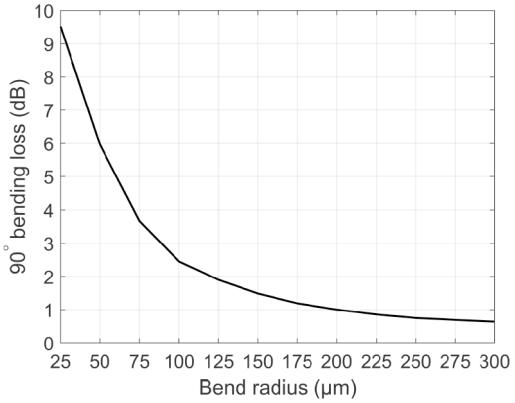

Fig. 9. The 90° bending loss for the ESM waveguide, simulated in 3D-FDTD.

These same building blocks could be used to achieve FTIR spectrometers similar to [2]. It should be noted that in some single-mode circuits individual multimode components (e.g. Euler bends or very low loss multimode waveguides) may well be desirable. In those cases care should be taken so that only the fundamental modes of those components are excited at their junctions with other components. ESM waveguides could be used to filter out light from any higher order modes that do get excited.

5. Conclusion

In this work, we have experimentally shown the well-known endlessly single-mode design approach for fibres can be applied to silicon photonics, as has been previously predicted theoretically [5]. We have demonstrated waveguides that support low-loss and single-mode propagation over the wavelength range 1.95 - 3.80 μm, covering an octave of frequency. To the best of our knowledge, this is the first experimental demonstration of endlessly single-mode behaviour in integrated photonics. We believe that this waveguide design approach can similarly be extended to longer wavelengths and different materials, overcoming a key challenge for MIR photonic devices that require a wide working bandwidth, particularly for chemical sensing applications.

Funding. Engineering and Physical Sciences Research Council (EP/N00762X/1, EP/N013247/1, EP/V047663/1); Royal Academy of Engineering (RF201617/16/33).

Disclosures. The authors declare no conflicts of interest.

Data availability. All data supporting this study are openly available from the University of Southampton repository in [22].

References

1. H. Lin, Z. Luo, T. Gu, L. C. Kimerling, K. Wada, A. Agarwal, and J. Hu, "Mid-infrared integrated photonics on silicon: a perspective," Nanophotonics **7**(2), 393–420 (2017).

Optics EXPRESS

2. M. C. M. M. Souza, A. Grieco, N. C. Frateschi, and Y. Fainman, "Fourier transform spectrometer on silicon with thermo-optic non-linearity and dispersion correction," Nat. Commun. **9**(1), 665 (2018).
3. R. Soref, J. Schmidtchen, and K. Petermann, "Large single-mode rib waveguides in GeSi-Si and Si-on-SiO_2," IEEE J. Quantum Electron. **27**(8), 1971–1974 (1991).
4. S. Pogossian, L. Vescan, and A. Vonsovici, "The single-mode condition for semiconductor rib waveguides with large cross section," J. Lightwave Technol. **16**(10), 1851–1853 (1998).
5. K. Bougot-Robin, J. P. Hugonin, M. Besbes, and H. Benisty, "Broad working bandwidth and "endlessly" single-mode guidance within hybrid silicon photonics," Opt. Lett. **40**(15), 3512–3515 (2015).
6. T. A. Birks, J. C. Knight, and P. S. J. Russell, "Endlessly single-mode photonic crystal fiber," Opt. Lett. **22**(13), 961–963 (1997).
7. R. Halir, P. J. Bock, P. Cheben, A. Ortega-Mo nux, C. Alonso-Ramos, J. H. Schmid, J. Lapointe, D.-X. Xu, J. G. Wangüemert-Pérez, Í. Molina-Fernández, and S. Janz, "Waveguide sub-wavlength structures: a review of principles and applications," Laser Photonics Rev. **9**(1), 25–49 (2015).
8. J. M. Luque-González, A. Herrero-Bermello, A. Ortega-Mo nux, I. Molina-Fernández, A. V. Velasco, P. Cheben, J. H. Schmid, S. Wang, and R. Halir, "Tilted subwavelength gratings: controlling anisotropy in metamaterial nanophotonic waveguides," Opt. Lett. **43**(19), 4691–4694 (2018).
9. S. M. Rytov, "Electromagnetic properties of a finely stratified medium," Soviet Physics JETP **2**, 466–475 (1956).
10. N. Hattasan, B. Kuyken, F. Leo, E. M. P. Ryckeboer, D. Vermeulen, and G. Roelkens, "High-Efficiency SOI Fiber-to-Chip Grating Couplers and Low-Loss Waveguides for the Short-Wave Infrared," IEEE Photonics Technol. Lett. **24**(17), 1536–1538 (2012).
11. M.-S. Rouifed, C. G. Littlejohns, G. X. Tina, Q. Haodong, T. Hu, Z. Zhang, C. Liu, G. T. Reed, and H. Wang, "Low Loss SOI Waveguides and MMIs at the MIR Wavelength of 2μm," IEEE Photonics Technol. Lett. **28**(24), 2827–2829 (2016).
12. J. S. Penadés, A. Z. Khokhar, M. Nedeljkovic, and G. Z. Mashanovich, "Low-Loss Mid-Infrared SOI Slot Waveguides," IEEE Photonics Technol. Lett. **27**(11), 1197–1199 (2015).
13. G. Z. Mashanovich, F. Y. Gardes, D. J. Thomson, Y. Hu, K. Li, M. Nedeljkovic, J. Soler Penadés, A. Z. Khokhar, C. J. Mitchell, S. Stankovic, R. Topley, S. A. Reynolds, Y. Wang, B. Troia, V. M. N. Passaro, C. G. Littlejohns, T. Dominguez Bucio, P. R. Wilson, and G. T. Reed, "Silicon Photonic Waveguides and Devices for Near- and Mid-IR Applications," IEEE J. Sel. Top. Quantum Electron. **21**(4), 407–418 (2015).
14. J. S. Penadés, A. Ortega-Mo nux, M. Nedeljkovic, J. G. Wangüemert-Pérez, R. Halir, A. Z. Khokhar, C. Alonso-Ramos, Z. Qu, I. Molina-Fernández, P. Cheben, and G. Z. Mashanovich, "Suspended silicon mid-infrared waveguide devices with subwavelength grating metamaterial cladding," Opt. Express **24**(20), 22908–22916 (2016).
15. B. Dong, X. Guo, C. P. Ho, B. Li, H. Wang, C. Lee, X. Luo, and G. Lo, "Silicon-on-Insulator Waveguide Devices for Broadband Mid-Infrared Photonics," IEEE Photonics J. **9**(3), 1–10 (2017).
16. R. Marchetti, C. Lacava, L. Carroll, K. Gradkowski, and P. Minzioni, "Coupling strategies for silicon photonics integrated chips," Photonics Res. **7**(2), 201–239 (2019).
17. J. C. Knight, T. A. Birks, P. S. J. Russell, and J. P. de Sandro, "Properties of photonic crystal fiber and the effective index model," J. Opt. Soc. Am. A **15**(3), 748–752 (1998).
18. M. Cherchi, S. Ylinen, M. Harjanne, M. Kapulainen, and T. Aalto, "Dramatic size reduction of waveguide bends on a micron-scale silicon photonic platform," Opt. Express **21**(15), 17814–17823 (2013).
19. C. J. Stirling, B. Guilhabert, W. Cao, K. S. Kiang, A. Z. Khokhar, M. Nedeljkovic, M. J. Strain, and G. Z. Mashanovich, "Investigations into group IV photonic waveguides with a wide working optical bandwidth," in *Silicon Photonics XV*, vol. 11285 G. T. Reed and A. P. Knights, eds., International Society for Optics and Photonics (SPIE, 2020), pp. 224–233.
20. D. González-Andrade, C. Lafforgue, E. Durán-Valdeiglesias, X. Le Roux, M. Berciano, E. Cassan, D. Marris-Morini, A. V. Velasco, P. Cheben, L. Vivien, and C. Alonso-Ramos, "Polarization- and wavelength-agnostic nanophotonic beam splitter," Sci. Rep. **9**(1), 3604 (2019).
21. C. J. Stirling, R. Halir, A. Sánchez Postigo, Z. Qu, J. Reynolds, J. Soler Penadés, G. Senthil Murugan, A. Ortega-Mo nux, J. G. Wangüemert-Pérez, I. Molína-Fernández, G. Z. Mashanovich, and M. Nedeljkovic, "Broadband 2×2 multimode interference coupler for mid-infrared wavelengths," Opt. Lett. **46**(21), 5300–5303 (2021).
22. C. J. Stirling, W. Cao, J. D. Reynolds, Z. Qu, T. D. Bradley, L. Mastronardi, F. Y. Gardes, and M. Nedeljkovic, "Dataset for: Mid-infrared silicon-on-insulator wavegudes with single-mode propagation over an octave of frequency,"University of Southampton, (2021). https://doi.org/10.5258/SOTON/D1827.